Fuel 371 (2024) 131868

Contents lists available at ScienceDirect

Fuel

journal homepage: www.elsevier.com/locate/fuel

Full Length Article

The interaction between NH_3 and CH_4 oxidation chemistry: A comprehensive study through combustion regimes and thermokinetic instabilities

Maria Virginia Manna, Raffaele Ragucci, Mara de Joannon, Pino Sabia *

Istituto di Scienze e Tecnologie per l'Energia e la Mobilità sostenibili – Consiglio Nazionale delle Ricerche, Napoli, Italy

ARTICLE INFO

Keywords:
Ammonia-methane oxidation
Oxidation regimes
Jet Stirred Reactor
NOx emissions

ABSTRACT

The present work explores the interaction between CH_4 and NH_3 oxidation chemistry, with particular focus on the effect of NH_3 on CH_4 oscillation regimes and nitrogen oxides emissions. Experimental tests were carried out in a Jet Stirred Flow Reactor, for fuel-lean CH_4-NH_3/O_2/N_2 mixtures, at fixed equivalence ratio (0.8), dilution level (90 %) and residence time (0.4 s), changing the inlet temperature and the fuel-mixture composition. Experimental results revealed a different influence of NH_3 on CH_4 oxidation depending on the NH_3 concentration in the fuel blend. In particular, mixture reactivity is slightly enhanced when NH_3 is increased from 0 up to 40 %, while reactants conversion is shifted to higher T_{in} for $NH_3 > 40$ %. Maps of instabilities were outlined for CH_4-NH_3 blends ranging from pure methane to pure ammonia. Both periodic and damped oscillations were detected, with different shapes, amplitudes and frequencies depending on the temperature and NH_3 concentration. Numerical results showed that the selected kinetic scheme reproduced the overall effect of NH_3 on mixture reactivity and NO emissions. Kinetic analyses suggested that the enhancing effect of NH_3 at relatively low temperatures is mainly ascribable to the formation of NO and its interaction with CH_3 radicals.

1. Introduction

The current energy crisis and the need to contain greenhouse gas emissions have driven research into alternative energy vectors to fossil fuels. The development of hydrogen-based combustion systems currently seems to be the predominant strategy, but the limitations of safe transport and storage, as well as the control of the high reactivity of hydrogen, are the main barriers to overcome [1]. Ammonia, as a hydrogen carrier and fuel itself, is attracting growing interest, due to century-long experience in its production, transport and storage, for its no-carbon nature and high octane number [2–4]. Nonetheless, at present, the use of pure ammonia as fuel seems still prohibitive in various applications due to its poor combustion properties (i.e. low laminar flame speed, low ignition delay time, high minimum ignition energy [2,4]) and the potential high emissions of fuel-NO_x [5]. For instance, the combustion of pure ammonia in traditional combustion systems is problematic due to stabilization issues and high concentrations of nitrogen oxides in the exhaust gases [2]. To reduce NO_x emissions, it is necessary to use abatement processes such as Selective Catalytic or Non-Catalytic Reduction (SCR or SNCR) [6–8] or rely on different combustion concepts like the two-stage combustion [9,10] or Mild combustion [11–14]. In particular, Sorrentino et al. [12] demonstrated that Mild combustion conditions can stabilize the oxidation of pure ammonia in a wider range of operating conditions, with very low NO_x formation.

Alternatively, the ammonia oxidation process can be improved through co-combustion strategies, adding more reactive species, like hydrogen [15–18], methane [19,20], diesel [21], gasoline [22,23], oxygenated fuels [24–30] to ammonia.

The interaction between ammonia and "fuel enhancers" oxidation chemistry can be explicated through promoting and inhibiting effects [31,32]. The enhancement of ammonia reactivity is governed by the increment of radical pools from the fast oxidation chemistry of the "fuel enhancers". On the other hand, the inhibiting effect may be related to the "OH scavenger" nature of ammonia [31,32]. Alzueta et al. [33] have recently studied the NH_3/CH_4 oxidation chemistry in a Laminar Flow Reactor, exploiting an enhancement of blend reactivity due fast methane conversion through the reaction $CH_4 + NH_2 = CH_3 + NH_3$. At the same time, Sabia et al. [32] have studied the oxidation behavior of NH_3/H_2 blends in a Jet Stirred Flow Reactor, demonstrating a mutual inhibiting

* Corresponding author.
E-mail address: pino.sabia@stems.cnr.it (P. Sabia).

https://doi.org/10.1016/j.fuel.2024.131868
Received 31 January 2024; Received in revised form 3 May 2024; Accepted 10 May 2024
Available online 19 May 2024

effect of ammonia and hydrogen oxidation chemistry due to the "OH scavenger" nature of ammonia and fast reconversion of NH_2 radicals to NH_3 through reaction $NH_2 + H_2 = NH_3 + H$.

In addition, ammonia may likely enhance the reactivity of hydrogen or carbon-based fuels releasing NO and NO_2, promoting the NO_x "sensitizing" chemistry. Many works from scientific literature have addressed this chemistry [34–39] doping simple hydrocarbons with NO and/or NO_2 or studying the co-oxidation of hydrocarbons with ammonia.

Recently, Arunthanayothin et al. [34] studied the co-oxidation of methane/ammonia through experimental tests in a Jet Stirred Flow Reactor (JSFR) and in a Flow Reactor (FR), for CH_4/NH_3 blends at different equivalence ratios. They found ammonia anticipates the onset of reactivity in fuel-lean conditions, with no effects for stoichiometric and fuel-rich conditions. Following kinetic analyses, they claimed that the major role in promoting methane oxidation was played by NO, even as an intermediate species in ammonia oxidation pathway. Indeed, the NO interacts with HO_2 radicals to produce NO_2 and OH, then the formed NO_2 reacts with CH_3 according to the reaction $CH_3 + NO_2 = CH_3O + NO$, thus promoting the system reactivity. Fuel-lean conditions favor the formation of HO_2 radicals and also NO_x from NH_3 oxidation, thus emphasizing the sensitizing effect of NO_x on the CH_4 chemistry.

NH_3-CH_4 mixtures oxidation in a JSFR was also studied by Jin et al. [40] at different equivalence ratios (0.5, 1, 2) and ammonia concentrations (0–100 %). The experimental results showed that at fuel-lean conditions, CO formation is postponed to higher temperatures as the NH_3 concentration increases, while this effect is not observed at stoichiometric and fuel-rich conditions. The authors reported a dual NO formation behavior. In particular, for temperatures lower than 1100 K, NO increases with the addition of NH_3 while for higher temperatures NO concentration is gradually reduced as the NH_3 concentration increases.

Bendtsen et al. [37] and Chan et al. [38] found that NO is more effective as a promoter of methane oxidation at low temperatures, while the enhancing effect of NO_2 overcomes that of NO at higher temperatures. Chan et al. [38] identified $CH_3O_2 + NO = CH_3O + NO_2$ and $CH_4 + NO_2 = CH_3 + HONO$ as the most sensitive reactions at low temperatures for NO and NO_2 respectively.

The NO/NO_2 sensitizing effect has to be properly addressed. Indeed, while literature evidence recognizes the improved performance of combustion systems fueled with ammonia blends compared to pure ammonia in terms of stability and thermal efficiency, NO_x emissions are generally increased due to the abundance of OH radicals, able to trigger the formation of fuel-NO_x from NH_3 oxidation pathways [19,20,41,42].

Understanding the chemical kinetics of ammonia-hydrocarbon blends is a prerequisite for the prediction of the combustion features and pollutant emissions of such mixtures in conventional and innovative combustion systems. Recently, due to the growing attention on CH_4-NH_3 oxidation, the amount of experimental data in model reactors [34,43] and kinetic mechanisms [5,34,43–46] describing their interaction is gradually increasing. Nevertheless, to the best of the authors' knowledge, the implications of the fuel mixture composition (i.e. the relative amount of CH_4 and NH_3) and temperature on reactivity, oxidation regimes and thermokinetic instabilities are not systematically discussed in the literature.

Therefore, the present work aims at investigating the effect of NH_3 on CH_4 oxidation through experimental tests in a Jet Stirred Flow Reactor, varying the concentration of ammonia in the fuel blend from 0 up to 100 %. A fuel-lean condition was exploited to emphasize the NO formation from ammonia oxidation. NO_x formation and system reactivity were analyzed at atmospheric pressure, at fixed residence time, ranging the preheating temperature from 800 up to 1300 K. Specific experimental tests were carried out to investigate instabilities and periodic oscillations as a function of ammonia concentration and operating temperature.

Simulations and kinetic analyses were performed with detailed kinetic mechanisms in order to interpret the experimental results and identify the main reaction pathways that control CH_4-NH_3 interaction at the various fuel concentrations.

2. Experimental and numerical tools

Experimental tests were performed in a Jet Stirred Flow Reactor (JSFR), changing parametrically the operating conditions. The JSFR consists of a quartz sphere with a volume of 113 cm^3, located within two semi-cylindrical electrically-heated fiber ovens, that allow to preheat the reactant mixture and control the ambient temperature, in order to minimize the heat losses. A detailed description of the experimental system can be found in the reference [47].

The concentrations of CH_4, O_2, N_2, H_2, CO, CO_2, C_2H_4, C_2H_6 were measured by a μ-gas-chromatograph (Agilent 3000), with maximum relative errors around ± 3 % (molar fraction). The μ-gas-chromatograph is equipped with two specific capillary columns: a column Plot U to detect carbon dioxide, ethylene, ethane and acetylene and a column Molsieve 5A to separate hydrogen, nitrogen, oxygen, methane and carbon monoxide. Species concentrations are quantified using a Thermal Conductivity Detector (TCD).

The NO concentration was detected by two analyzers (TESTO 350 and ABB AO2020 equipped with two UV channels). The error for NO emissions is ± 2 ppm in the range of 0–99.9 ppm, and ± 5 % in the range of 100–500 ppm. The concentrations of the species are reported on dry basis since the water in the exhaust gases is retained by a silica gel trap located downstream of the reactor outlet. The experiments were replicated three times in different days, with a maximum error of 5 % on the species concentrations and ± 5 K on the temperature.

The temperature inside the reactor was measured by two thermocouples (N-type, R-type). The R-type is an unshielded thermocouple with a fast response time (less than 30 ms) and a precision of ± 0.25 %. The temperature signal is detected by a National Instruments module with an acquisition rate of 90 samples per second for each channel that allows to record the fast temperature variation during oscillations.

The operating conditions explored are summarized in Table 1.

Experiments were performed for CH_4-NH_3/O_2 mixtures diluted in N_2, keeping constant the dilution level (d = 90 %) and the residence time ($\tau = 0.4$ s), while changing the inlet temperature within the range T_{in} = 800–1300 K. The NH_3 content was increased from 0 up to 100 %, with an increment of 10 %, while the equivalence ratio was fixed at 0.8. In particular, a fuel-lean condition was exploited to emphasize the NO formation from ammonia oxidation.

The experimental tests were carried out at atmospheric pressure (p = 1.16 atm).

The experimental results were simulated with the PSR code of CHEMKIN PRO [48] using different detailed kinetic mechanisms [5,34,45,49,50], selected from the numerical investigations carried out by Jin et al. [40] and Yin et al. [51]. The system was modeled as non-adiabatic with an estimated global heat transfer coefficient equal to 1.7 10^{-3} cal/(cm^2 s K), according to the criteria discussed in [47].

The kinetic mechanisms considered for the numerical investigations are listed in Table 2. Among them, the model named "NH_3-CH_4_2023" was built-up merging the NH_3 oxidation chemistry model developed by Manna et al. [52] and the C-sub-mechanism from the detailed kinetic scheme by Shrestha et al. [44]. The NH_3-submodel was optimized based on NH_3 and NH_3-NO speciation in JSFR at relatively low working

Table 1
Experimental operative conditions.

Conditions	Range
Inlet temperature (T_{in})	800–1300 K
Equivalence ratio (Φ)	0.8
NH_3 in the fuel-blend	0–100 %
Dilution level (d)	90 % in N_2
Residence time (τ)	0.4 s
Pressure	1.16 atm

Table 2
Kinetic mechanisms and validating conditions.

Mechanism	Validating conditions
NH_3-CH_4_2023 (p.w.) [44,52]	Several facilities and operative conditions (JSFR experiments, laminar flame speed, flow reactors, ignition delay time).
Okafor et al. [45]	Laminar flame speed for CH_4-NH_3 mixtures at various NH_3 concentrations and mixture equivalence ratio (0.8–1.3), at 298 K and 0.10 MPa.
Glarborg et al. [5]	Low-pressure (35 Torr) flame, for near equimolar ammonia-oxygen mixtures.
Wang et al. [50]	Laminar burning velocities of NH_3/CH_3OH/air and NH_3/C_2H_5OH/air, at atmospheric pressure and varying the equivalence ratio and the mixing ratio.
Arunthanayothin et al. [34]	Several facilities and operative conditions (JSFR experiments, laminar flame speed, flow reactors, ignition delay time).

temperatures (900–1300 K) and further tested against several literature data (ignition delay time, laminar flame speed and flow reactors), with good results for stoichiometric and fuel lean conditions. The model was developed by revising the NH_3 mechanism of Shrestha et al. [44], considering recent updated rate constants for NO formation and reduction pathways [53–55] and including a new reaction subset for diazene [56], both crucial for ammonia low-temperature oxidation chemistry, in particular for the prediction of H_2 and NO. Furthermore, NH_3 collisional efficiency for all third-body reactions is declared in the model. The role of NH_3 as a strong collider in third-body reaction was discussed in detail by Sabia et al. [29] and underlined by recent studies of Glarborg et al. [57] and Jasper et al. [58].

For the sake of briefness, given the similarity of the investigated conditions with the work [52] (speciation in JSFR, under lean conditions at 90 % dilution level), only the numerical outcomes obtained with the "NH_3-CH_4_2023" model will be presented below, while the mechanism predictions for the other schemes are illustrated in the Supplementary Material, Section C.

3. Experimental results

3.1. Temperature and species for the oxidation of CH_4-NH_3 mixtures

Fig. 1 shows the experimental reactor temperature increment (ΔT), CH_4, H_2 and NO concentrations as a function of the inlet temperature (T_{in}) for the oxidation of CH_4-NH_3 mixtures diluted in N_2. For completeness, the concentration profiles of other stable species (CO_2, CO, C_2H_4, C_2H_6) are reported in the Supplementary Material, Section A.

In each figure, the empty symbols represent conditions where periodic temperature (and species) oscillations were detected, thus each plotted value has to be considered averaged in time.

According to the temperature and CH_4 profiles (Fig. 1a, 1b), the oxidation of pure methane (black squares) starts for $T_{in} > 1080$ K. The onset of reactivity is characterized by periodic instabilities that persist in the temperature range $T_{in} = 1090$–1140 K, in agreement with previous experimental findings [59], then they disappear for higher temperatures, where the complete reactant conversion is achieved. The maximum measured ΔT is equal to 85 K for $T_{in} > 1170$ K. The mixture with only methane is herein considered as the reference case.

The addition of a small concentration of NH_3 (10 %-light blue diamonds) drastically enhances the mixture reactivity: the onset of the oxidation process is shifted to $T_{in} = 970$ K, thus it is anticipated of about 150 K with respect to the reference case. This behavior is in agreement with the experimental evidence by Arunthanayothin et al. [34].

Instabilities are detected in the temperature range $T_{in} = 1050$–1100

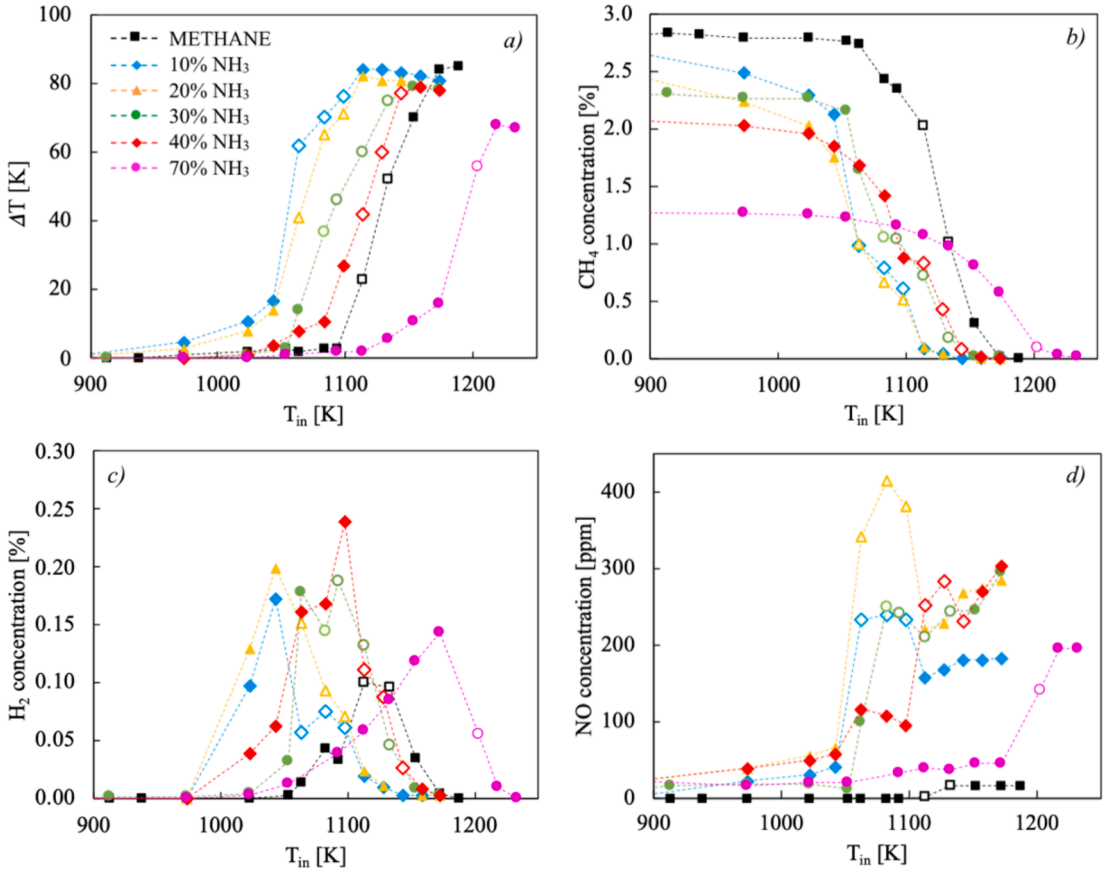

Fig. 1. Experimental temperature and species profiles vs T_{in} for the oxidation of CH_4-NH_3 mixtures for NH_3 concentrations ranging from 0 to 70 %, at $\phi = 0.8$, $\tau = 0.4$ s and $P = 1.16$ atm.

K, while for higher T_{in} steady-state conditions are achieved.

The enhancing effect of NH_3 on CH_4 oxidation persists for greater NH_3 contents, nonetheless it becomes less strong as the NH_3 concentration increases, as suggested by the ΔT and species profiles at 20 % (orange triangles), 30 % (green circles) and 40 % (red diamonds) of NH_3. In particular, at 40 % NH_3, the system reactivity is almost equal to the one exhibited by pure methane.

For NH_3 concentrations greater than 40 %, the reactivity of the mixtures becomes lower with respect to the pure CH_4 case. Indeed, the onset of reactivity for the mixture containing 70 % NH_3 (pink circles) occurs at $T_{in} = 1130$ K, thus postponed by about 50 K with respect to the base case.

The maximum ΔT at steady state conditions decreases as the NH_3 concentration increases, consistently with the lower heating value of the fuel-blend.

Oscillatory behaviors are established for all the explored mixture compositions. It can be observed that the onset temperature for the dynamic regimes changes with the NH_3 content in the mixture, congruently with the onset of reactivity. For $NH_3 < 40$ %, temperature oscillations are detected for a range of T_{in} (ΔT_{oscill}) equal to 50 K, whereas this range tightens for higher NH_3 concentrations. A detailed discussion of the oscillatory behavior is reported in the next paragraph.

As a further indicator of system reactivity, H_2 concentration is reported (Fig. 1c). In general, the H_2 trend is non-monotonic for all the considered CH_4-NH_3 mixtures. In the case of pure methane, H_2 has a peak of 0.1 % at about $T_{in} = 1110$ K. As the NH_3 concentration increases, the maximum is shifted to lower T_{in}, consistently with mixture reactivity, and its value decreases down from 0.2 % at 10 % NH_3 to 0.15 % at 70 % NH_3.

Regarding NO emissions (Fig. 1d), for pure methane, NO concentration is negligible (<15 ppm) within the considered temperature range. NO formation increases as NH_3 is fed to the system. For instance, at steady state conditions at high temperatures, for $NH_3 = 10$ %, NO concentration is about 150–180 ppm. The highest NO emissions are then detected for mixtures with $NH_3 = 20$–40 %, with NO concentrations equal to about 230 ppm and 300 ppm, respectively. Following, for $NH_3 = 70$ %, NO emissions decrease to about 190 ppm, almost reaching the NO_x emissions detected for $NH_3 = 10$ %.

3.2. Maps of oxidation regimes for CH_4-NH_3 mixtures

The identification of the oxidation regimes was scrupulously carried out by means of further experimental tests, parametrically changing NH_3 concentration from 0 to 100 % with a step of 10 %, and T_{in} in the range of 1000–1300 K with a small increment (ΔT_{in}) of 10 K, while preserving mixture equivalence ratio (ϕ) and dilution levels (d) (ϕ = 0.8 and d = 90 %, respectively). To this aim, the reactor temperature (T_r) was recorded over time. The results of such experimental tests are summarized in a NH_3%-T_{in} map (Fig. 2).

The light-blue region identifies the "Low Temperature" regime, where a steady state condition with a low temperature increment (ΔT = 10–15 K) is achieved. Below this region, no reactivity is observed. The dark-red area delimitates conditions where periodic temperature oscillations were detected, while within the light-red area the system working temperature evolves towards a steady state condition passing through damped temperature oscillations in time. An example of the experimental temperature profile in the case of periodic and damped oscillations is reported in the figure inset.

Above the damped oscillation region, the oxidation process occurs with full reactant conversion and maximum temperature increment (high-temperature combustion regime) without oscillatory transient behaviors.

In agreement with Fig. 1, the map indicates that the oxidation of pure methane starts at about 1080 K and for T_{in} = 1090–1140 K periodic oscillations are detected. Afterward, the oxidation process evolves through damped oscillations for $T_{in} > 1140$ K, that disappear for $T_{in} > 1170$ K. Therefore, the width of the periodic oscillation range ($\Delta T_{in,osc}$) is almost 50 K, while the damped oscillations range ($\Delta T_{in,damp}$) is wide about 30 K. For NH_3 concentrations lower than 30 %, the onset of both periodic and damped oscillations is shifted to lower T_{in} than pure methane, in particular, the mixture with $NH_3 = 10$ % exhibits dynamic regimes at the lowest $T_{in} = 1050$ K. Nonetheless, $\Delta T_{in,osc}$ and $\Delta T_{in,damp}$ are not affected by NH_3, until $NH_3 < 30$ %. The periodic oscillations region becomes narrower for $NH_3 > 30$ % and the lower temperature boundary is shifted to higher T_{in} as the NH_3 concentration increases. For $NH_3 > 70$ %, periodic instabilities are no longer detected, while it is still possible to observe damped oscillations, also for the pure ammonia mixture.

The characteristic frequency of the oscillations varies between 0.5 and 3 Hz, depending on the T_{in} and NH_3 concentration in the fuel mixture. In case of pure methane, the frequency ranges from 0.5 to 2 Hz. The mixtures with lower NH_3 concentrations (10, 20 %) show oscillations with the highest frequency, about 3 Hz, while for $NH_3 > 20$ %, the frequency changes in the range of 0.5–1.5 Hz.

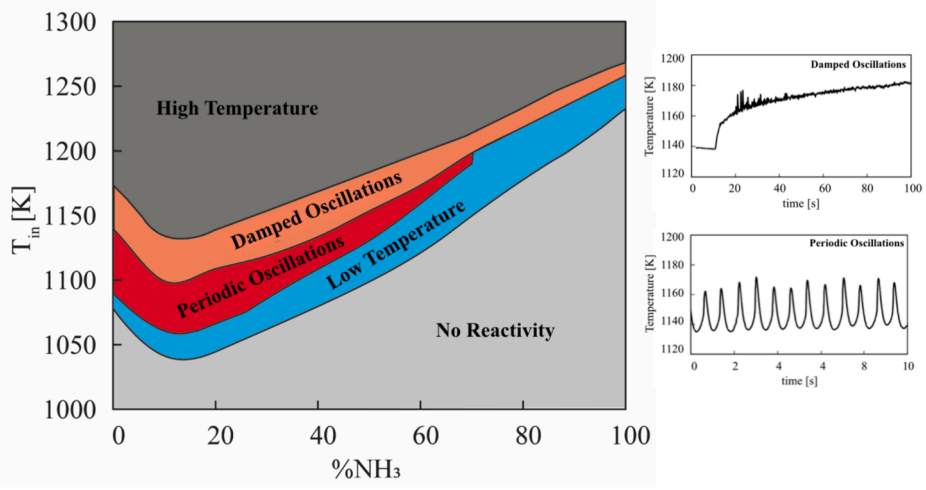

Fig. 2. Maps of oxidation regimes and experimental temperature profiles in case of damped and periodic oscillations. Damped oscillations and periodic oscillations profiles in time refer to a mixture with 20 % NH_3 at $T_{in} = 1140$ K and $T_{in} = 1090$ K, respectively.

4. Kinetic analyses and discussion

4.1. Simulations with detailed kinetic mechanisms

The kinetic mechanism NH_3-CH_4_2023 was tested against the experimental data previously presented. Fig. 3 shows the numerical predictions and the experimental data for ΔT, CH_4, H_2 and NO concentrations while the simulations of CO_2, CO, C_2H_4, C_2H_6 are reported in Supplementary Material, Section B.

Solid lines represent conditions where a steady state is achieved, while the dashed lines qualitatively identify periodic solutions.

Temperature and CH_4 concentration profiles indicate that the mechanism well reproduces the reactivity of the mixtures, in particular the promoting effect of NH_3 for NH_3 = 10–20 % and the retarding effect in the case of NH_3 = 70 %. The model suggests that mixtures with 30–40 % have similar reactivity to the pure methane oxidation. Also the dynamic region is reproduced by the mechanism with a good degree of accuracy ($\Delta T_{in,osc}$ is predicted with an error of ± 10 K). Further details on the simulations of oscillation regions are provided below.

The H_2 concentration is satisfactorily predicted at NH_3 = 0, 10, 70 %, while the model underestimates its formation for T_{in} < 1100 K at NH_3 = 20 %-40 %.

Regarding the formation of NO, in general, the model reproduces NO trends for all the NH_3 contents.

Some discrepancies are observed for the prediction of NO for NH_3 concentrations in the range 20–40 %, since the mechanism overestimates NO emissions in the low-temperature region and underestimates them in the high temperature one. A better agreement is observed at NH_3 content equal to 10 % and 70 %.

The simulation of the instabilities map is illustrated in Fig. 4. For each NH_3 concentrations, the inlet temperatures corresponding to both oscillation onset and end were identified, in order to outline the low- and the high-temperature boundary of the map, respectively. The model prediction is then plotted against the experimental data, in particular the experimental data are reported as red area, while the simulated map is overlapped as a dashed green area.

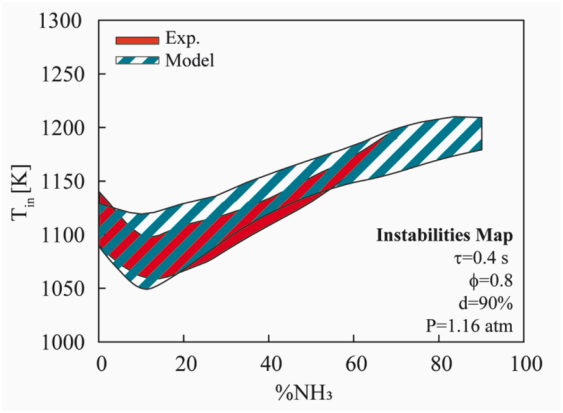

Fig. 4. Experimental and numerical maps of oscillations as a function of NH_3 concentration and inlet temperature (T_{in}).

Among the considered models, the kinetic mechanism NH_3-CH_4_2023 provides a better prediction of the instabilities map. The comparison with the other schemes is reported in the Supplementary Material.

In the case of pure CH_4, the model well reproduces the T_{in} range where instabilities occur (1100–1120 K). The numerical oscillation area extends in a wider NH_3 concentration range compared with the experimental data, indeed the model suggests that instabilities disappear for

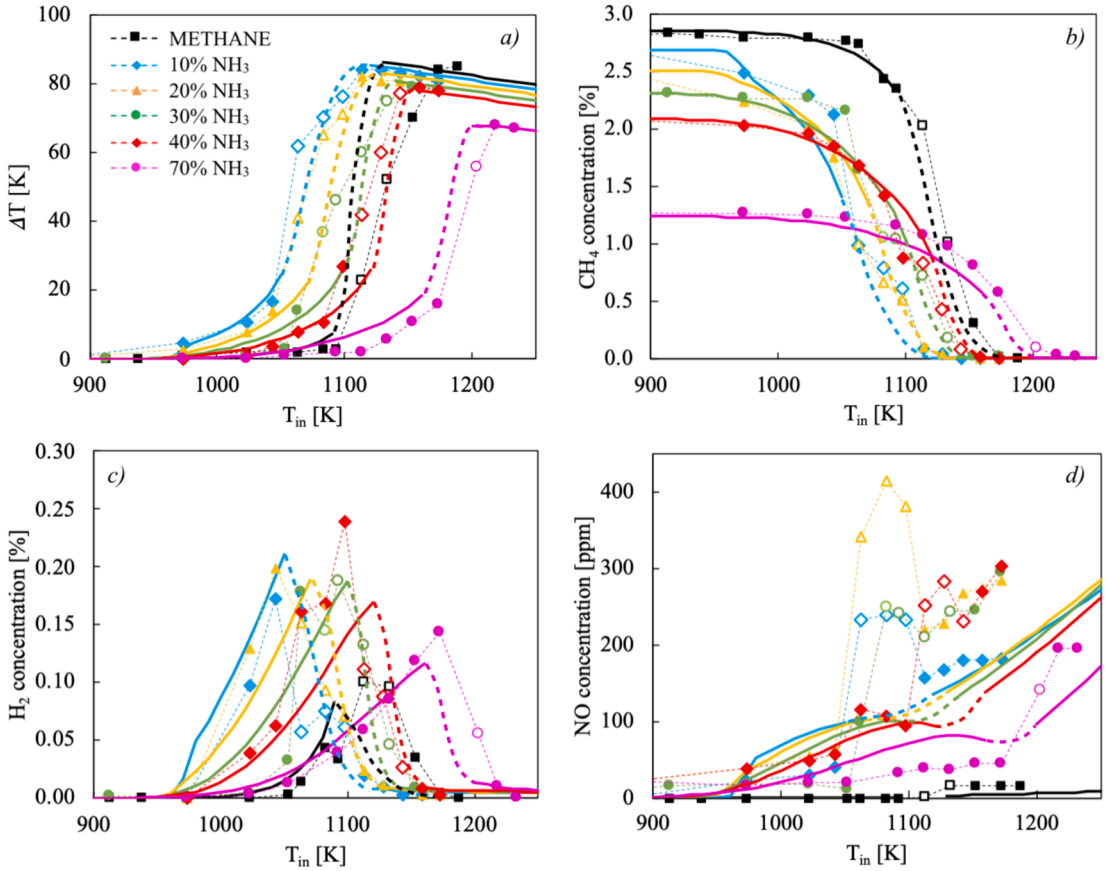

Fig. 3. Numerical predictions with NH_3-CH_4_2023 model and experimental results as a function of T_{in} for NH_3 = 0, 10, 20, 30, 40, 70 %.

$NH_3 > 90$ %. The shape of the dynamic behaviors map is reproduced by the model, however, the calculated boundaries do not match perfectly the experimental data, in particular, for NH_3 = 20–60 %, the model suggests oscillations establish and disappear at lower T_{in} with respect to the experimental data. In general, the error varies in the range 5–20 K. According to the model, the oscillations frequency ranges in a wider range than the experimental one. Indeed, in case of pure methane oxidation, the oscillation frequency increases with T_{in} from 0.2 up to 33 Hz. For the CH_4-NH_3 mixtures the frequency varies in the range 0.5–20 Hz, in particular the frequency decreases as the NH_3 concentration increases.

It is worth highlighting that these oscillations have a thermo-kinetic nature [31,59,60]. The fundamental aspect of thermokinetic oscillatory behaviors involves a negative feedback mechanism, where both temperature and reaction products impact the ignition stages, hindering the runaway acceleration typical of the explosion process, based on positive feedback. The negative feedback is caused by competitive reaction pathways, chain-branching and chain terminating, that have comparable reaction rates within this specific temperature range [31,59,61,62].

Indeed, these instabilities mark the evolution from the low-temperature oxidation regime to the high-temperature one, characterized by a variation of the main kinetic pathways.

Therefore, the accurate prediction of such phenomenology is challenging and requires a delicate balance between the most sensitive reactions that control the oxidation process during this transition.

4.2. Methane-ammonia oxidation chemistry

The experimental and numerical results agree on the effect of NH_3 on CH_4 oxidation, in particular low ammonia concentrations (<40 %) have a promoting effect on the fuel-blend oxidation with respect to pure methane, while the mixture with 70 % of NH_3 ignites at higher T_{in}. In addition, results suggest that the temperature range (in particular, the minimum T_{in} of the $\Delta T_{in,osc}$ range) for the occurrence of instabilities can vary significantly depending on NH_3 concentration.

In order to identify the major reaction steps and any interaction between CH_4 and NH_3, reaction rates and flux diagrams analyses were performed. For the path flux analysis, two extreme conditions were chosen, specifically the mixture with 10 % and 90 % of NH_3, since they have the highest and lowest reactivity with respect to methane, respectively, as suggested by the simulations reported previously.

The kinetic analyses were performed at the point of 10 % and 100 % fuel consumption for both the mixtures, which in terms of inlet temperatures means 1020 K and 1300 K at NH_3 = 10 % and 1150 K and 1300 K at NH_3 = 90 %. Both the N- and C- pathways were studied.

The CH_4-NH_3 oxidation pathways at $NH_3 = 10$ % are shown in Fig. 5. At low temperatures (Fig. 5a), the CH_4 is dehydrogenated to CH_3 according to the reaction $CH_4 + OH = CH_3 + H_2O$. Then, two main consumption routes occur: the oxidation of CH_3 via $CH_3 \rightarrow CH_3O \rightarrow CH_2O \rightarrow HCO \rightarrow CO$ ($CH_3 + NO_2 = CH_3O + NO$ and $CH_3O + M = CH_2O + O + M$ or $CH_3 + O_2 = CH_2O + OH$, $CH_2O + OH = HCO + H_2O$, $HCO + O_2 = CO + HO_2$) and the recombination to $C_2H_6 \rightarrow C_2H_5 \rightarrow C_2H_4$ ($CH_3 + CH_3 + M = C_2H_6 + M$, $C_2H_6 + OH = C_2H_5 + H_2O$, $C_2H_5 + M = C_2H_4 + H + M$). Under these operative conditions, $CH_3 + NO_2 = CH_3O + NO$ represents the only cross-reaction between the C-species and N-species and it is the main CH_3 consumption reaction. The formation of NO_2 depends on the NH_3 oxidation pathways, which starts with the formation of NH_2 via $NH_3 + OH = NH_2 + H_2O$ and proceeds through the sequence: $NH_2 \rightarrow H_2NO \rightarrow HNO \rightarrow NO \rightarrow NO_2$.

The reaction rate of $NH_3 + OH = NH_2 + H_2O$ is five times lower than $CH_4 + OH = CH_3 + H_2O$, suggesting that the oxidation process is kinetically controlled by the C-species reactions. Nevertheless, although slow, the formation of NO and thus NO_2 as intermediates of NH_3 reaction pathway is responsible for the greater reactivity of the mixture than in the case of pure methane. The NO and NO_2 are involved in a "catalytic loop", that promotes the reactivity due to the formation of OH radicals

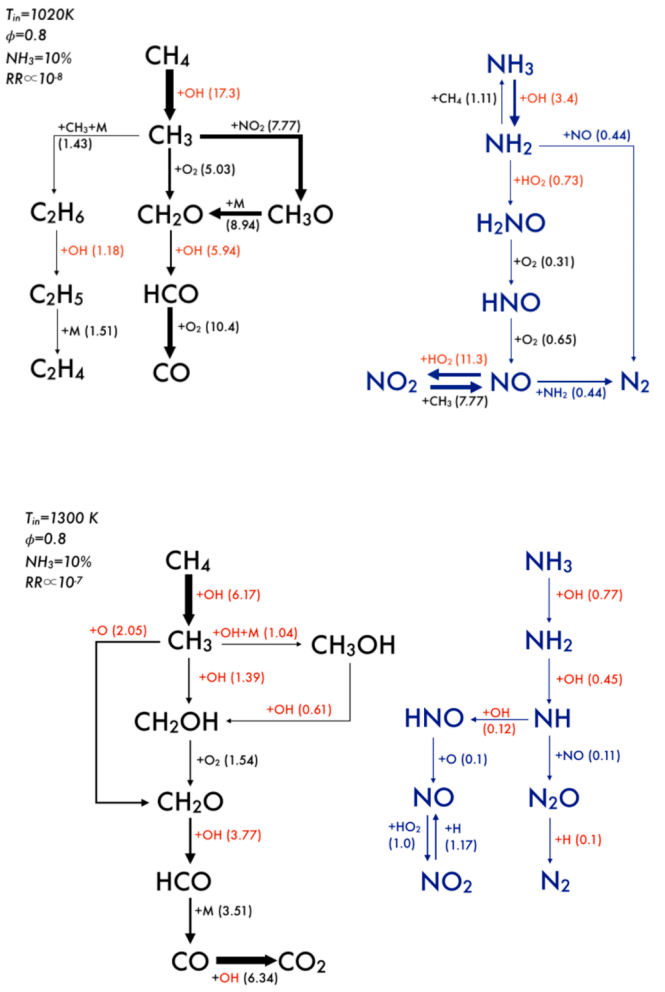

Fig. 5. CH_4 and NH_3 oxidation pathways with $NH_3 = 10$ %, at $T_{in} = 1020$ K and $T_{in} = 1300$ K, $\tau = 0.4$ s, $\phi = 0.8$, p = 1.16 atm.

via the reaction $NO + HO_2 = NO_2 + OH$ and converts CH_3 to CH_3O via $CH_3 + NO_2 = CH_3O + NO$, regenerating NO.

Increasing the temperature, the CH_4 and NH_3 pathways progress almost independently, as shown in Fig. 5b. Regarding CH_4 oxidation, the recombination route to C_2H_6 becomes negligible since the dominant CH_3 reactions are the formation of CH_2O via $CH_3 + OH = CH_2O + H_2$ and the formation of CH_2OH according to $CH_3 + OH = CH_2OH + H$. CH_3OH is also formed via $CH_3 + OH(+M) = CH_3OH(+M)$. The methanol pathways reconnect to the main one through the reactions $CH_3OH \rightarrow CH_2OH \rightarrow CH_2O$.

Also the reaction pathway of NH_3 changes as the temperature increases. The NH_2 is dehydrogenated to NH by OH radicals, then NH is converted to HNO or N_2O. The former is responsible for the formation of NO via $HNO + O = NO + OH$, the latter is converted to N_2 according to the reaction $N_2O + H = N_2 + OH$. NO and NO_2 are still involved in a loop since NO is oxidized to NO_2 via $NO + HO_2 = NO_2 + OH$ and NO_2 is reconverted to NO reacting with H ($NO_2 + H = NO + OH$), thus without C-species contribution. In general, the mechanism suggests that there are no cross-reactions between C-species and N-species at high temperatures for such fuel-mixture composition. The only interaction between carbon and nitrogen chemistry is represented by the competition for the OH radicals consumption ($CH_4 + OH = CH_3 + H_2O$ and $NH_3 + OH = NH_2 + H_2O$), that are mainly produced by the reaction $H + O_2 = OH + O$.

The CH_4 and NH_3 oxidation pathways at NH_3 = 90 % is shown in Fig. 6.

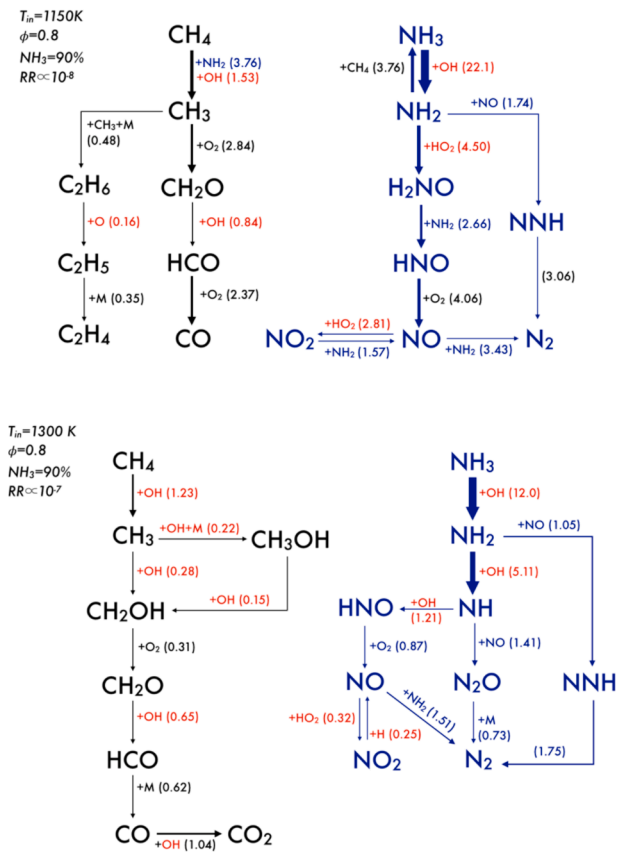

Fig. 6. CH_4 and NH_3 oxidation pathways with NH_3 = 90 %, at T_{in} = 1150 K and T_{in} = 1300 K, τ = 0.4 s, ϕ = 0.8, p = 1.16 atm.

At low temperatures, the CH_4 and NH_3 oxidation proceeds through similar reaction pathways to the case with 10 % NH_3, nevertheless two crucial points must be highlighted. First, the cross-reaction $CH_4 + NH_2 = CH_3 + NH_3$ between the fuel molecules represents the main interaction between the C- and N-pathways. According to this reaction, the NH_2 radicals extract H from CH_4, promoting the CH_3 conversion but, at the same time, this reaction reconverts back the NH_2 to NH_3. Second, even though NO is still involved in the reaction $NO + HO_2 = NO_2 + OH$, other competitive routes (i.e. $DeNO_x$ reactions) reduce the NO to N_2, thus decreasing the reaction rates of the former reaction and reducing its effectiveness as a promoter of the overall system reactivity. In addition, the reaction $NO_2 + CH_3 = NO + CH_3O$ is overcome by $NO_2 + NH_2 = NO + H_2NO$, therefore the NO-NO_2 loop does not involve the C-chemistry at NH_3 = 90 %.

At higher temperatures, the cross-reaction $CH_4 + NH_2 = CH_3 + NH_3$ becomes marginal, thus the CH_4 and NH_3 oxidation routes proceed independently through pathways similar to those discussed at 10 % NH_3.

A further interpretation of the interaction between methane and ammonia and the accelerating or inhibiting effect of ammonia on methane kinetics is provided by the rate of formation and consumption reactions of OH radicals. OH Reaction Rates (RRs) were analyzed as a function of temperature, within the Low-Temperature regime, for various NH_3 concentrations, in particular NH_3 = 0, 10, 40, 90 %. The condition at NH_3 = 40 % was analyzed as it exhibits a similar reactivity to pure methane, as suggested by the simulations and experimental data illustrated in Fig. 2. Results are reported in Fig. 7.

In case of methane oxidation (Fig. 7a), the OH radicals are mainly consumed to produce CH_3 and HCO radicals, according to the reactions $CH_4 + OH = CH_3 + H_2O$ and $CH_2O + OH = HCO + H_2O$ respectively. The formation of OH is dependent on CH_3 reactions, in particular $CH_3 + O_2 = CH_2O + OH$ and $CH_3 + HO_2 = CH_3O + OH$, and on the H_2O_2 decomposition ($H_2O_2 + M = 2OH + M$), while the typical high temperature branching reaction $H + O_2 = OH + O$ plays a marginal role for low-temperature conditions. In other words, the OH formation at low temperatures and fuel-lean conditions depends on HO_2 radical, which directly reacts with CH_3 to produce OH or recombines to H_2O_2.

The role of HO_2 reactions is emphasized as the NH_3 concentration increases. Indeed, the formation of NO from NH_3 oxidation pathway enables the reaction $NO + HO_2 = NO_2 + OH$, that is the main reaction producing OH radicals.

The RR of such reaction is one order of magnitude greater than the ones active in case of pure methane oxidation (i.e. $CH_3 + O_2 = CH_2O + OH$ or $CH_3 + HO_2 = CH_3O + OH$), while the H_2O_2 decomposition is marginal (not reported in the figure), since the HO_2 radicals are mainly involved in $NO + HO_2 = NO_2 + OH$ instead of recombine to H_2O_2.

Therefore, the NO-NO_2 loop is responsible for the increased reactivity of the mixture at NH_3 = 10 %.

Although this remains true for increasing ammonia concentrations, it must be emphasized that the promoting effect of the NO-NO_2 loop is counterbalanced by the inhibiting competition between methane and ammonia for OH-radical consumption, as reported in Fig. 7c and d.

At NH_3 = 40 % the reaction $NH_3 + OH = NH_2 + H_2O$ is faster than $CH_4 + OH = CH_3 + H_2O$, but the RRs of such reactions are comparable and the overall oxidation behavior of the mixture is similar to the pure methane one. At NH_3 = 90 %, the RR of $NH_3 + OH = NH_2 + H_2O$ is considerably larger than $CH_4 + OH = CH_3 + H_2O$ and this difference is emphasized as the temperature increases. Therefore, the oxidation process is controlled by the NH_3 oxidation pathways, resulting in a slowdown of the overall combustion kinetics of the mixture. In addition, also the role of NO as reactivity booster becomes less relevant, since competitive NO reactions (i.e. DeNOx reactions) occur as the NH_3 concentration increases.

For high temperatures, C- and N-chemistry compete for the OH radical consumption. Fig. 8 shows the main OH Reaction Rates at fixed T_{in} = 1300 K, as a function of the NH_3 concentration in the mixture. It is possible to observe that the role of C-chemistry becomes gradually less important as ammonia concentration increases. Indeed, for $NH_3 < 50$ %, the reactions $CH_4 + OH = CH_3 + H_2O$ and $CO + OH = CO_2 + H$ are the main OH consumption routes, while for higher NH_3 concentration, the reactions $NH_3 + OH = NH_2 + H_2O$ and $NH_2 + OH = NH + H_2O$ act as OH scavenger, slowing down the mixture reactivity.

5. Conclusions

The oxidation features of diluted CH_4-NH_3 mixtures were experimentally and numerically studied in a Jet Stirred Flow Reactor as a function of the inlet temperature, parametrically changing the concentration of NH_3 in the fuel blend ranging from 0 to 70 % and keeping constant the mixture equivalence ratio, dilution level and residence time. Speciation at steady state conditions and dynamic behaviors were systematically analyzed.

The experimental results showed that the onset of reactivity is shifted to lower temperatures with respect to pure methane in case of $NH_3 < 40$ %, suggesting that low concentrations of NH_3 can have a promoting effect on the mixture reactivity. Specifically, at NH_3 = 10 % the ignition of the mixture occurs at about 970 K, while pure methane oxidation starts at 1080 K. The enhancing effect of NH_3 becomes less strong as the NH_3 concentration increases and vanishes for $NH_3 > 50$ %, since the ignition of mixtures with higher NH_3 concentration occurs at higher inlet temperatures as the NH_3 content increases. Adding low concentrations of NH_3 also boosts NO formation with respect to pure methane oxidation. The highest NO emissions were measured for mixtures with NH_3 = 20–40 %, while the mixture with NH_3 = 70 % produced the lowest NO emissions among the explored fuel blends.

Damped and periodic oscillations were mapped for pure methane and methane-ammonia mixtures, as a function of the temperature and NH_3 concentration. It was observed that the width of the periodic

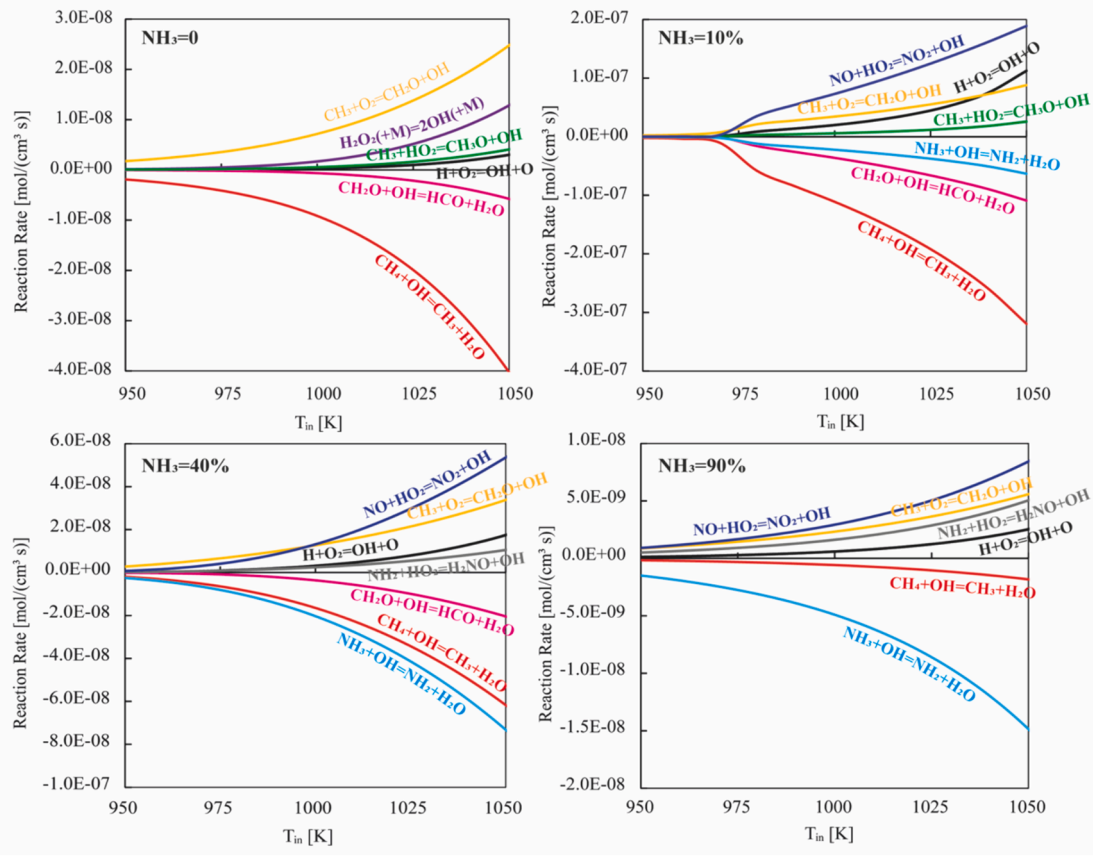

Fig. 7. OH Reaction Rate as a function of the inlet temperature at different NH_3 concentrations (NH_3 = 0, 10, 40, 90 %).

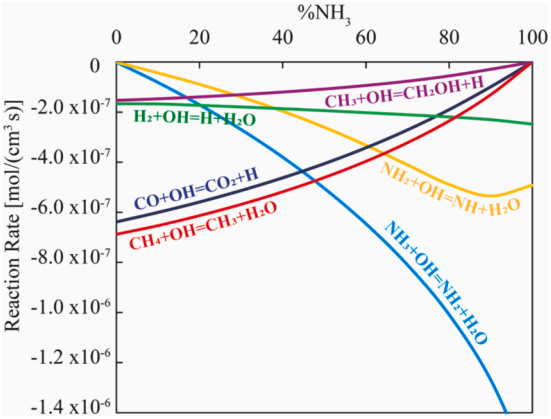

Fig. 8. OH Reaction Rate as a function of the NH_3 concentrations at fixed T_{in} = 1300 K.

oscillation range ($\Delta T_{in,osc}$) is almost 50 K for pure methane oxidation and it is not affected by NH_3, until NH_3 < 30 %, while the periodic oscillations region becomes narrower for NH_3 > 30 % and for NH_3 > 70 %, periodic instabilities are no longer detected.

The mechanism selected for the simulations was able to reproduce the overall effect of NH_3 on CH_4 oxidation and dynamic regimes. Flux diagrams and reaction rate analyses showed that, at low temperatures and for low ammonia concentrations, the enhancing effect of N-chemistry on CH_4 oxidation can be attributed to the interaction of NO and NO_2 with the HO_2/OH radical pool and the methyl radical. Indeed, once NO is formed from NH_3 oxidation, it reacts with HO_2 radical producing the more reactive OH, according to the reaction $NO + HO_2 = NO_2 + OH$. Then, the formed NO_2 is reconverted back to NO, reacting with CH_3 according to the reaction $CH_3 + NO_2 = CH_3O + NO$, which also promotes the oxidation of CH_3 via the CH_3O channel.

As the NH_3 concentration increases, competitive DeNOx reactions occur, limiting the promoting effect of $NO + HO_2 = NO_2 + OH$. For these conditions, the cross-reaction $CH_4 + NH_2 = CH_3 + NH_3$ becomes relevant, but its effectiveness as promoter of CH_4 oxidation is lower than the NO-NO_2 loop. In addition, it must be highlighted that CH_4 and NH_3 compete for OH consumption according to the reactions $CH_4 + OH = CH_3 + H_2O$ and $NH_3 + OH = NH_2 + H_2O$, respectively. As NH_3 concentration increases above 50 %, the reaction rate of $NH_3 + OH = NH_2 + H_2O$ overcomes $CH_4 + OH = CH_3 + H_2O$, therefore, the oxidation chemistry is controlled by the slower NH_3 oxidation pathways, causing the slowdown of the overall oxidation process. Moreover, since the onset of the oxidation process is shifted to higher temperatures, HO_2 radicals play a limited role in system reactivity and, consequently, the sensitizing effect of the NO-NO_2 loop loses its effectiveness.

CRediT authorship contribution statement

Maria Virginia Manna: Writing – original draft, Methodology, Investigation, Conceptualization. **Raffaele Ragucci:** Writing – review & editing, Supervision. **Mara de Joannon:** Writing – review & editing, Supervision, Conceptualization. **Pino Sabia:** Writing – review & editing, Supervision, Investigation, Conceptualization.

Declaration of competing interest

The authors declare that they have no known competing financial interests or personal relationships that could have appeared to influence the work reported in this paper.

Data availability

Data is available as Supplementary Material

Acknowledgements

The authors gratefully acknowledge the partial financial support of the European Union—NextGeneration EU in the framework of the "National PNRR - AdP MiTE-ENEA" M2C2 "Ricerca e sviluppo sull'idrogeno".

The authors gratefully acknowledge the partial financial support of the European Union, NextGenerationEU - in the framework of the National Sustainable Mobility Center - MOST, CN00000023, Italian Ministry of University and Research Decree n. 1033— 17/06/2022, Spoke 12, CUP B43C22000440001.

Appendix A. Supplementary material

Supplementary data to this article can be found online at https://doi.org/10.1016/j.fuel.2024.131868.

References

[1] Abdin Z, Zafaranloo A, Rafiee A, Mérida W, Lipiński W, Khalilpour KR. Hydrogen as an energy vector. Renew Sustain Energy Rev 2020:120. https://doi.org/10.1016/j.rser.2019.109620.
[2] Kobayashi H, Hayakawa A, Somarathne KDKA, Okafor EC. Science and technology of ammonia combustion. Proc Combust Inst 2019;37:109–33. https://doi.org/10.1016/j.proci.2018.09.029.
[3] Salmon N, Bañares-Alcántara R. Green ammonia as a spatial energy vector: A review. Sustain Energy Fuels 2021;5:2814–39. https://doi.org/10.1039/d1se00345c.
[4] Valera-Medina A, Amer-Hatem F, Azad AK, Dedoussi IC, de Joannon M, Fernandes RX, et al. Review on ammonia as a potential fuel: from synthesis to economics. Energ Fuels 2021;35:6964–7029. https://doi.org/10.1021/acs.energyfuels.0c03685.
[5] Glarborg P, Miller JA, Ruscic B, Klippenstein SJ. Modeling nitrogen chemistry in combustion. Prog Energy Combust Sci 2018;67:31–68. https://doi.org/10.1016/j.pecs.2018.01.002.
[6] Klippenstein SJ, Harding LB, Glarborg P, Miller JA. The role of NNH in NO formation and control. Combust Flame 2011;158:774–89. https://doi.org/10.1016/j.combustflame.2010.12.013.
[7] Tayyeb Javed M, Irfan N, Gibbs BM. Control of combustion-generated nitrogen oxides by selective non-catalytic reduction. J Environ Manage 2007;83:251–89. https://doi.org/10.1016/j.jenvman.2006.03.006.
[8] Asghar U, Rafiq S, Anwar A, Iqbal T, Ahmed A, Jamil F, et al. Review on the progress in emission control technologies for the abatement of CO2, SOx and NOx from fuel combustion. J Environ Chem Eng 2021;9:106064. https://doi.org/10.1016/j.jece.2021.106064.
[9] Kurata O, Iki N, Inoue T, Matsunuma T, Tsujimura T, Furutani H, et al. Development of a wide range-operable, rich-lean low-NOx combustor for NH 3 fuel gas-turbine power generation. Proc Combust Inst 2019;37:4587–95. https://doi.org/10.1016/j.proci.2018.09.012.
[10] Lee T, Guahk YT, Kim N, Lee H, Lee MJ. Stability and emission characteristics of ammonia-air flames in a lean-lean fuel staging tangential injection combustor. Combust Flame 2023;248:112593. https://doi.org/10.1016/j.combustflame.2022.112593.
[11] Cavaliere A, De Joannon M. Mild combustion. Prog Energy Combust Sci 2004;30:329–66. https://doi.org/10.1016/j.pecs.2004.02.003.
[12] Sorrentino G, Sabia P, Bozza P, Ragucci R, de Joannon M. Low-NOx conversion of pure ammonia in a cyclonic burner under locally diluted and preheated conditions. Appl Energy 2019;254:1–7. https://doi.org/10.1016/j.apenergy.2019.113676.
[13] Ariemma GB, Sabia P, Sorrentino G, Bozza P, De JM, Ragucci R. Influence of water addition on MILD ammonia combustion performances and emissions. Proc Combust Inst 2020;000:1–8. https://doi.org/10.1016/j.proci.2020.06.143.
[14] Sabia P, Sorrentino G, Ariemma GB, Manna MV, Ragucci R, de Joannon M. MILD Combustion and Biofuels : A Minireview. Energ Fuels 2021;35:19901–19. https://doi.org/10.1021/acs.energyfuels.1c02973.
[15] Lhuillier C, Brequigny P, Lamoureux N, Contino F, Mounaïm-Rousselle C. Experimental investigation on laminar burning velocities of ammonia/hydrogen/air mixtures at elevated temperatures. Fuel 2020;263:116653. https://doi.org/10.1016/j.fuel.2019.116653.
[16] Hayakawa A, Goto T, Mimoto R, Arakawa Y, Kudo T, Kobayashi H. Laminar burning velocity and Markstein length of ammonia/air premixed flames at various pressures. Fuel 2015;159:98–106. https://doi.org/10.1016/j.fuel.2015.06.070.
[17] Li J, Huang H, Kobayashi N, He Z, Nagai Y. Study on using hydrogen and ammonia as fuels: Combustion characteristics and NOx formation. Int J Energy Res 2014;38:1214–23. https://doi.org/10.1002/er.3141.
[18] Valera-Medina A, Pugh DG, Marsh P, Bulat G, Bowen P. Preliminary study on lean premixed combustion of ammonia-hydrogen for swirling gas turbine combustors. Int J Hydrogen Energy 2017;42:24495–503. https://doi.org/10.1016/j.ijhydene.2017.08.028.
[19] Valera-Medina A, Marsh R, Runyon J, Pugh D, Beasley P, Hughes T, et al. Ammonia–methane combustion in tangential swirl burners for gas turbine power generation. Appl Energy 2017;185:1362–71. https://doi.org/10.1016/j.apenergy.2016.02.073.
[20] Ariemma GB, Sorrentino G, Ragucci R, de Joannon M, Sabia P. Ammonia/Methane combustion: Stability and NOx emissions. Combust Flame 2022;241:112071. https://doi.org/10.1016/j.combustflame.2022.112071.
[21] Reiter AJ, Kong SC. Combustion and emissions characteristics of compression-ignition engine using dual ammonia-diesel fuel. Fuel 2011;90:87–97. https://doi.org/10.1016/j.fuel.2010.07.055.
[22] Kobayashi H, Hayakawa A, Somarathne KDKA, Okafor EC, Lubrano Lavadera M, Sabia P, et al. Ammonia and gasoline fuel blends for spark ignited internal combustion engines. Combust Flame 2009;3:319–33. https://doi.org/10.1016/j.combustflame.2017.06.021.
[23] Haputhanthri SO, Austin C, Maxwell T, Fleming J. Ammonia and gasoline composite liquid fuel blends emulsified with ethanol and methanol for direct displacement in internal combustion engines. IOSR Journal of Mechanical and Civil Engineering 2014;11:11–8. https://doi.org/10.9790/1684-11241118.
[24] Lu M, Dong D, Wei F, Long W, Wang Y, Cong L, et al. Chemical mechanism of ammonia-methanol combustion and chemical reaction kinetics analysis for different methanol blends. Fuel 2023;341:127697. https://doi.org/10.1016/j.fuel.2023.127697.
[25] Issayev G, Giri BR, Elbaz AM, Shrestha KP, Mauss F, Roberts WL. Combustion behavior of ammonia blended with diethyl ether. Proc Combust Inst 2021;38:499–506. https://doi.org/10.1016/j.proci.2020.06.337.
[26] Cai T, Zhao D. Enhancing and assessing ammonia-air combustion performance by blending with dimethyl ether. Renew Sustain Energy Rev 2022;156:112003. https://doi.org/10.1016/j.rser.2021.112003.
[27] Dai L, Hashemi H, Glarborg P, Gersen S, Marshall P, Mokhov A, et al. Ignition delay times of NH3/DME blends at high pressure and low DME fraction : RCM experiments and simulations. Combust Flame 2021;227:120–34. https://doi.org/10.1016/j.combustflame.2020.12.048.
[28] Xu H, Wang J, Zhang C, Dai L, He Z, Wang Q. Numerical study on laminar burning velocity of ammonia flame with methanol addition. Int J Hydrogen Energy 2022;47:28152–64. https://doi.org/10.1016/j.ijhydene.2022.06.111.
[29] Brackmann C, Methling T, Lavadera ML, Capriolo G, Konnov AA. Experimental and modeling study of nitric oxide formation in premixed methanol + air flames. Combust Flame 2020;213:322–30. https://doi.org/10.1016/j.combustflame.2019.11.043.
[30] Gross CW, Kong S. Performance characteristics of a compression-ignition engine using direct-injection ammonia – DME mixtures. Fuel 2013;103:1069–79. https://doi.org/10.1016/j.fuel.2012.08.026.
[31] Manna MV, Sabia P, Sorrentino G, Viola T, Ragucci R, de Joannon M. New insight into NH3-H2 mutual inhibiting effects and dynamic regimes at low-intermediate temperatures. Combust Flame 2022;243:111957. https://doi.org/10.1016/j.combustflame.2021.111957.
[32] Sabia P, Manna MV, Ragucci R, de Joannon M. Mutual inhibition effect of hydrogen and ammonia in oxidation processes and the role of ammonia as "strong" collider in third-molecular reactions. Int J Hydrogen Energy 2020;45:32113–27. https://doi.org/10.1016/j.ijhydene.2020.08.218.
[33] Alzueta MU, Abián M, Elvira I, Mercader VD, Sieso L. Unraveling the NO reduction mechanisms occurring during the combustion of NH3/CH4 mixtures. Combust Flame 2022::112531. https://doi.org/10.1016/j.combustflame.2022.112531.
[34] Arunthanayothin S, Stagni A, Song Y, Herbinet O, Faravelli T, Battin-Leclerc F. Ammonia-methane interaction in jet-stirred and flow reactors: An experimental and kinetic modeling study. Proc Combust Inst 2021;38:345–53. https://doi.org/10.1016/j.proci.2020.07.061.
[35] Song Y, Marrodán L, Vin N, Herbinet O, Assaf E, Fittschen C, et al. The sensitizing effects of NO 2 and NO on methane low temperature oxidation in a jet stirred reactor. Proc Combust Inst 2019;37:667–75. https://doi.org/10.1016/j.proci.2018.06.115.
[36] Dagaut P. On the Oxidation of Ammonia and Mutual Sensitization of the Oxidation of No and Ammonia: Experimental and Kinetic Modeling. Combust Sci Technol 2019;00:1–13. https://doi.org/10.1080/00102202.2019.1678380.
[37] Bendtsen AB, Glarborg P, Dam-Johansen K. Low temperature oxidation of methane: The influence of nitrogen oxides. Combust Sci Technol 2000;151:31–71. https://doi.org/10.1080/00102200008924214.
[38] Chan YL, Barnes FJ, Bromly JH, Konnov AA, Zhang DK. The differentiated effect of NO and NO2 in promoting methane oxidation. Proc Combust Inst 2011;33:441–7. https://doi.org/10.1016/j.proci.2010.05.029.
[39] Li P, Li W, Wang K, Hu F, Ding C, Guo J, et al. Experiments and kinetic modeling of NO reburning by CH4 under high CO2 concentration in a jet-stirred reactor. Fuel 2020;270:117476. https://doi.org/10.1016/j.fuel.2020.117476.
[40] Jin S, Tu Y, Liu H. Experimental study and kinetic modeling of NH3/CH4 co-oxidation in a jet-stirred reactor. Int J Hydrogen Energy 2022;47:36323–41. https://doi.org/10.1016/j.ijhydene.2022.08.178.
[41] Xiao H, Valera-Medina A, Bowen PJ. Study on premixed combustion characteristics of co-firing ammonia/methane fuels. Energy 2017;140:125–35. https://doi.org/10.1016/j.energy.2017.08.077.
[42] Filipe Ramos C, Rocha RC, Oliveira PMR, Costa M, Bai XS. Experimental and kinetic modelling investigation on NO, CO and NH3 emissions from NH3/CH4/air

premixed flames. Fuel 2019;254:115693. https://doi.org/10.1016/j.fuel.2019.115693.
[43] Mendiara T, Glarborg P. Ammonia chemistry in oxy-fuel combustion of methane. Combust Flame 2009;156:1937–49. https://doi.org/10.1016/j.combustflame.2009.07.006.
[44] Shrestha KP, Lhuillier C, Barbosa AA, Brequigny P, Contino F, Mounaïm-Rousselle C, et al. An experimental and modeling study of ammonia with enriched oxygen content and ammonia/hydrogen laminar flame speed at elevated pressure and temperature. Proc Combust Inst 2021;38:2163–74. https://doi.org/10.1016/j.proci.2020.06.197.
[45] Okafor EC, Naito Y, Colson S, Ichikawa A, Kudo T, Hayakawa A, et al. Experimental and numerical study of the laminar burning velocity of CH4–NH3–air premixed flames. Combust Flame 2018;187:185–98. https://doi.org/10.1016/j.combustflame.2017.09.002.
[46] Szanthoffer AG, Zsély IG, Kawka L, Papp M, Turányi T. Testing of NH3/H2 and NH3/syngas combustion mechanisms using a large amount of experimental data. Appl Energy Combust Sci 2023:14. https://doi.org/10.1016/j.jaecs.2023.100127.
[47] Manna MV, Sabia P, Ragucci R, de Joannon M. Oxidation and pyrolysis of ammonia mixtures in model reactors. Fuel 2020;264:116768. https://doi.org/10.1016/j.fuel.2019.116768.
[48] CHEMKIN-PRO 15131, Reaction Design: San Diego, 2013.
[49] Okafor EC, Somarathne KDKA, Hayakawa A, Kudo T, Kurata O, Iki N, et al. Towards the development of an efficient low-NOx ammonia combustor for a micro gas turbine. Proc Combust Inst 2019;37:4597–606. https://doi.org/10.1016/j.proci.2018.07.083.
[50] Wang Z, Han X, He Y, Zhu R, Zhu Y, Zhou Z, et al. Experimental and kinetic study on the laminar burning velocities of NH3 mixing with CH3OH and C2H5OH in premixed flames. Combust Flame 2021;229:111392. https://doi.org/10.1016/j.combustflame.2021.02.038.
[51] Yin G, Xiao B, Zhan H, Hu E, Huang Z. Chemical kinetic study of ammonia with propane on combustion control and NO formation. Combust Flame 2023:249. https://doi.org/10.1016/j.combustflame.2023.112617.
[52] Manna MV, Sabia P, Shrestha KP, Seidel L, Ragucci R, Mauss F, et al. NH3NO interaction at low-temperatures: An experimental and modeling study. Proc Combust Inst 2022;000:1–10. https://doi.org/10.1016/j.proci.2022.09.027.
[53] Stagni A, Cavallotti C, Arunthanayothin S, Song Y, Herbinet O, Battin-Leclerc F, et al. An experimental, theoretical and kinetic-modeling study of the gas-phase oxidation of ammonia. React Chem Eng 2020;5:696–711. https://doi.org/10.1039/c9re00429g.
[54] Song S, Hanson RK, Bowman CT, Golden DM, Chavarrio Cañas JE, Monge-Palacios M, et al. Shock tube determination of the overall rate of NH2 + NO → products at high temperatures. Proc Combust Inst 2022;32:2163–74. https://doi.org/10.1016/j.combustflame.2021.111708.
[55] Chavarrio Cañas JE, Monge-Palacios M, Zhang X, Sarathy SM. Probing the gas-phase oxidation of ammonia: Addressing uncertainties with theoretical calculations. Combust Flame 2021::111708. https://doi.org/10.1016/j.combustflame.2021.111708.
[56] Marshall P, Rawling G, Glarborg P. New reactions of diazene and related species for modelling combustion of amine fuels. Mol Phys 2021;119:17–8. https://doi.org/10.1080/00268976.2021.1979674.
[57] Glarborg P, Hashemi H, Cheskis S, Jasper AW. On the rate constant for NH2+HO2and third-body collision efficiencies for NH2+H(+M) and NH2+NH2(+M). J Phys Chem A 2021;125:1505–16. https://doi.org/10.1021/acs.jpca.0c11011.
[58] Jasper AW. Predicting third-body collision efficiencies for water and other polyatomic baths. Roy Soc Ch 2022;238:68–86. https://doi.org/10.1039/d2fd00038e.
[59] Lubrano Lavadera M, Song Y, Sabia P, Herbinet O, Pelucchi M, Stagni A, et al. Oscillatory Behavior in Methane Combustion: Influence of the Operating Parameters. Energ Fuels 2018;32:10088–99.
[60] Manna MV, Sabia P, Ragucci R, de Joannon M. Ammonia oxidation regimes and transitional behaviors in a Jet Stirred Flow Reactor. Combust Flame 2021;228:388–400. https://doi.org/10.1016/j.combustflame.2021.02.014.
[61] Sabia P, Manna MV, Cavaliere A, Ragucci R, de Joannon M. Ammonia oxidation features in a Jet Stirred Flow Reactor. The role of NH2 chemistry. Fuel 2020;276:118054. https://doi.org/10.1016/j.fuel.2020.118054.
[62] Sabia P, de Joannon M. On H2–O2 oxidation in several bath gases. Int J Hydrogen Energy 2020;45:8151–67. https://doi.org/10.1016/j.ijhydene.2020.01.134.